Use of an Embedded Contact Sensor to Study Nanoscale Heat Transfer in Heat Assisted Magnetic Recording

Haoyu Wu[1, a)] and David Bogy[1]

University of California at Berkeley, Berkeley, CA, 94720

(Dated: 5 January 2017)

A near field transducer (NFT) is employed in the heat assisted magnetic recording (HAMR) technology in order to focus the light energy into a nanoscale spot on the disk. This is necessary to heat the high coercivity magnetic media to its Curie temperature so the write transducer can record data. However, the heat transfer mechanism across the head disk interface (HDI) is still not well understood. The current perpendicular media recording (PMR) systems have a thermal fly-height control (TFC) means in the air bearing slider near the read/write transducers for placing the transducers within 1 to 2 nm of the rotating disk. In order to monitor this near contact spacing, this system also uses an embedded contact sensor (ECS). Here we investigate how this ECS can be used to study the heat transfer across the nanoscale gap between the read/write transducer and the disk. This study shows that the self heating effect of the ECS is strong when its current bias is too high. But this self heating effect can be isolated from other heat sources, which allows us to use the ECS for the desired heat transfer measurements.. The experiments show that the heat transfer across the HDI is a strong function of the head-disk spacing.

Keywords: HAMR, heat transfer, HDD, nano technology

[a)] wuhaoyu@berkeley.edu

The hard disk drive (HDD) is still the dominant technology in digital data storage due to its cost efficiency and long term reliability compared with other forms of data storage devices. The HDDs are widely used in personal computing, gaming devices, cloud services, data centers, surveillance, etc. Because the super paramagnetic limit of perpendicular media recording (PMR) has been reached at the data density of about $1\,\mathrm{Tb/in^2}$, heat assisted magnetic recording (HAMR) is being pursued and is expected to help increase the areal density to over $10\,\mathrm{Tb/in^2}$ in HDDs in order to fulfill future worldwide data storage demands.[1–3] In HAMR, the magnetic media is heated locally ($\sim 50\,\mathrm{nm} \times 50\,\mathrm{nm}$) and momentarily ($\sim 1\,\mathrm{ns}$) to its Curie temperature ($\sim 450\,^{\circ}\mathrm{C}$) by a laser energy source that is focused by a near field transducer (NFT). The design temperature of the NFT is much lower than the media's Curie temperature. As a result, the heat can flow back from the media to the NFT. This is called the back-heating effect. Since the distance between the NFT and the media is only a couple of nanometers, the back-heating effect could be very strong and cause undesired additional temperature increase on the NFT, shortening its lifetime.

Therefore, understanding the heat transfer between the media and the NFT is very important for improving its reliability. Recent studies include several aspects, including the NFT self-heating effect, disk temperature profile, heat transfer across the head disk interface (HDI), etc. The NFT self-heating effect has been studied often, both numerically and experimentally, and several efforts have been made to reduce it.[4–8] Besides, the disk temperature profile, the change of lubricant and carbon overcoat due to the heating were also intensively investigated.[9–11] The heat transfer across the HDI has historically been predicted by the air bearing model,[12] which holds for most cases when the temperature difference in the HDI is small. However, it only considers the air convection heat transfer mechanism and may not be applicable when a significant amount of conduction and radiation occurs. Recently, a phonon tunneling model was established to predict the nanoscale heat transfer. It was pointed out that the correlations between two surfaces cannot be neglected when the distance between the two surfaces is within the range of the wavelength of the radiation and it can make a major contribution to the heat transport.[13–15] Some numerical and experimental studies have also been performed to examine the model.[16,17]

The embedded contact sensor (ECS) was developed by the industry to detect the head disk contact during near contact operation.[18–20] The sensor is temperature sensitive and therefore it can be used to assist studying the heat transfer between the disk and the NFT.

However, the sensor itself is not well understood and some uncertainties of its working principle still exist.

In this paper, we experimentally study the ECS currently found in advanced HDD systems. We first introduce the basic techniques developed in HDDs and their roles in the experiment. Then the experimental procedure is discussed and the results are presented. This is followed by the discussion and conclusion.

The Thermal Fly-height Control (TFC) technique was developed in order to adjust the distance between the read/write transducer and the disk, which is the minimum clearance point between the head and the disk, also called head-disk spacing (d_{HD}), bringing it from $\sim$10 nm down to less than 1 nm.[21] In the TFC system, a resistive heater is embedded in the trailing edge of the slider near the read/write transducer. When the heater is supplied with current, it generates heat due to the Joule heating effect. It heats up the surrounding material, causing local thermal expansion inside the slider. The expansion results in the protrusion on the slider surface, lowering d_{HD}. Meanwhile, the local temperature of the slider also rises. This effect is called TFC heating.

As mentioned above, the ECS was developed by the industry to detect the head disk contact. It is a resistor made of temperature sensitive material. Its resistance changes with its temperature. The ECS is nominally 1 to 2 µm wide, 0.2 to 0.5 µm high and 20 to 60 nm thick but it can vary with the design of the head. The ECS is located on the air bearing surface (ABS) of the flying head, between the slider's reader and writer. Therefore, it is also at the minimum clearance point, and can sense the frictional heating caused by the head-disk contact. What's more, when there is TFC heating, the ECS senses the heat from the TFC heater. A schematic diagram of the TFC heater and the ECS is shown in Fig. 1.

The relation between its resistance and its temperature can be expressed as

$$R_E(T_E) = R_{E0}\,(1 + \alpha_{T0}\,(T_E - T_0)) \tag{1}$$

where $R_E(T_E)$ and R_{E0} are the resistances of the ECS at any ECS temperature T_E and room temperature T_0; α_{T0} is the temperature coefficient of resistance at T_0. To determine α_{T0}, we put the ECS head in an isolated environmental chamber with temperature control. An ohmmeter and a thermometer were used to measure the resistance of the ECS and its surrounding temperature simultaneously. The result of the measurement yielded $\alpha_{T0} = 3.5 \times 10^{-3}\,\mathrm{K}^{-1}$.

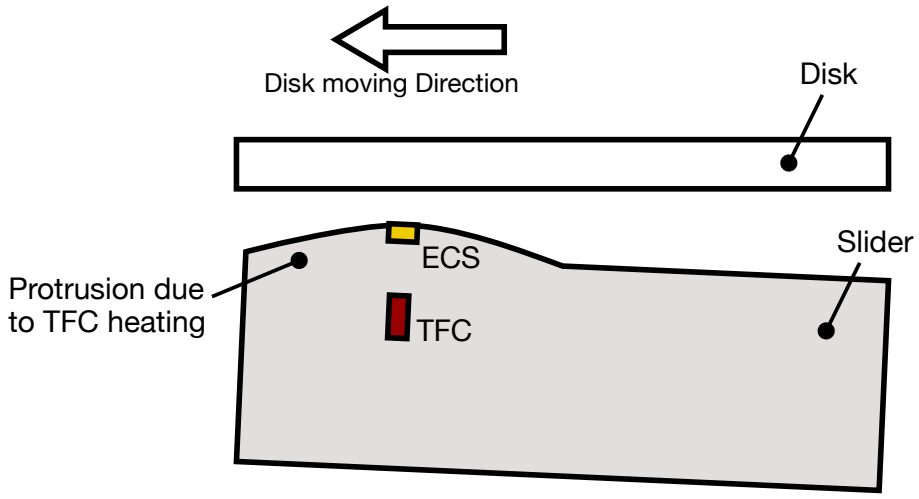

FIG. 1: A schematic diagram of the TFC heater and the ECS in the slider. The heater is embedded inside the slider while the ECS is on the surface of the slider. Powering on the TFC heater leads to the protrusion of the slider, lowers the fly height. It also heats the local region. Schematic not to scale.

Since the ECS is very sensitive to electrostatic shock, R_E is usually measured by a voltmeter-ammeter method, where a constant current bias (I_E) is applied through the ECS, the voltage of ECS (V_E) is measured and the resistance R_E is calculated using Ohm's law ($R_E = V_E/I_E$). Then the temperature increase of the ECS ($\theta_E = T_E - T_0$) can be calculated based on Eq. (1). However, since the ECS is also a resistor, applying the bias current through it will cause an additional Joule heating effect, which is sensed by the ECS. This is called ECS self heating. As a result, θ_E is a combination of the TFC heating and the ECS self heating. Since there are no explicit nonlinear factors, this is expressed as:

$$\theta_E = \theta_E^E + \theta_E^T \tag{2}$$

where θ_E^E is the ECS temperature increase due to ECS self heating and θ_E^T is the ECS temperature increase due to TFC heating.

An ECS-TFC heating experiment was designed in order to study the ECS self heating effect. In the experiment, 2.5-inch PMR disks with glass substrate were used on a rotation speed controlled spindle. The head with the embedded TFC heater and the ECS was flying on the disk. An acoustic emission (AE) sensor was used for head-disk contact detection.

Initially, the power of the TFC heater, also called TFC power (P_T), was set to zero. The head was flying on the disk passively. In this case, the ECS is only heated by itself. In other

words, there is no TFC heating but only ECS heating, and $\theta_E = \theta_E^E$. Therefore, by changing I_E and measuring θ_E, the temperature increase due to ECS self heating can be obtained. In the experiment, I_E was selected as 0.5 mA, 1 mA, 1.5 mA and 2 mA. The corresponding R_E was measured and converted to θ_E according to Eq. (1). Then the electric power supplied to the ECS (P_E) was calculated based on Joule's Law, i.e., $P_E = I_E^2 R_E$.

The relation between θ_E and P_E when the head is flying passively is shown in Fig. 2. It can be seen that θ_E is a linear function of P_E. This is because in the passive-fly status, there is no TFC heating, ECS is the only heat source. This leads to a simple linear heat transfer problem, in which the temperature field is linear with the power density of the sole heat source. The slope of the curve is defined as the ECS self heating rate with the value 200.2 K/mW. This agrees with published simulation results.[18] It can also be seen that $\theta_E = 4.6$ K when $I_E = 0.5$ mA (or $P_E = 0.028$ mW) but $\theta_E = 124.8$ K when $I_E = 2$ mA (or $P_E = 0.637$ mW). This means that if I_E is sufficiently low, θ_E^E is minimal and can be neglected, while that is not the case if I_E is too high. It is also to be noticed that the experiment was done for various disk rotation speeds (ω), selected from 3000 RPM, 4000 RPM and 5000 RPM. Each data point in Fig. 2 consists of three points taken at the three different speeds overlapping with each other. This means that ω has no effect on R_E and θ_E when the head is passively flying. This is because when the head is far enough away ($d_{HD} > 2$ nm) from the disk, the heat transfer change across the HDI is so small that it does not affect θ_E.

After the passive-fly experiment, the TFC heater was powered on to adjust d_{HD}. When the head was flying on the disk, P_T was increased from 0 mW in steps of 0.25 mW. The increase of P_T causes the decrease of d_{HD}, in which 1 mW increase of P_T causes about 0.1 nm decrease of d_{HD}. This relation between P_T and d_{HD} is essentially linear down to a proximity condition where there is some strong increase in the heat transfer between the slider and the disk.[22,23] Head-disk contact happened when $d_{HD} = 0$, which was detected by the AE sensor. Then P_T was reset to zero. As in the passive-fly experiment, various ω were used, selected from 3000 RPM, 4000 RPM and 5000 RPM. Different values of I_E were applied to the ECS, and R_E was obtained and converted to θ_E. Also, the value of I_E was selected from 0.5 mA, 1 mA, 1.5 mA and 2 mA.

Fig. 3 shows the experimental results. Figs. 3(a)(b)(c) show the AE sensor signal versus TFC power, P_T, with ω of 5000 RPM, 4000 RPM and 3000 RPM, respectively. Each plot

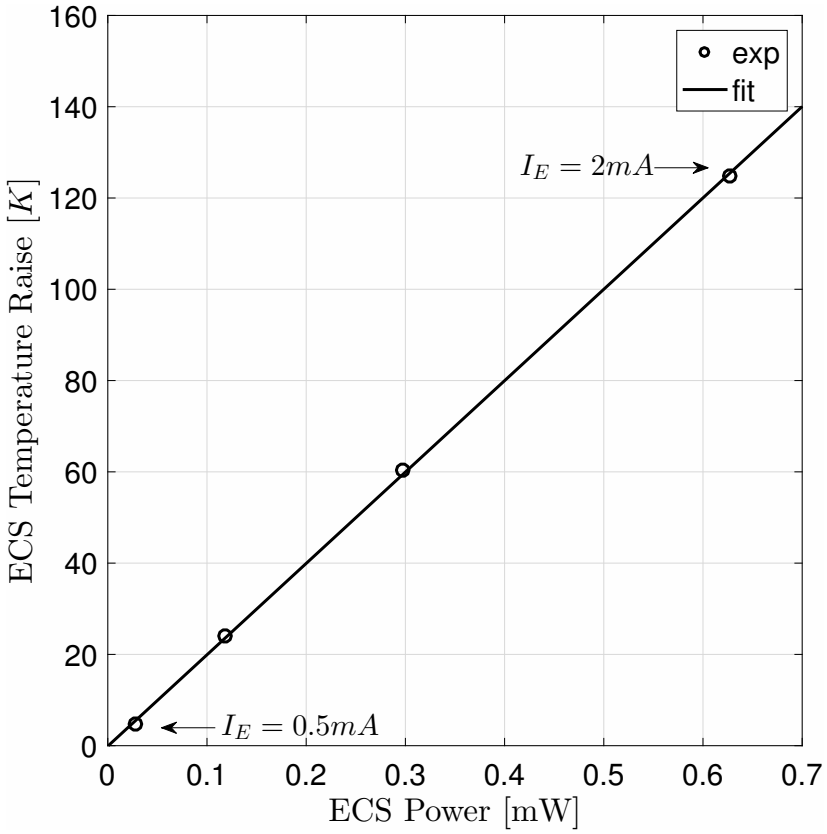

FIG. 2: The dependence of the ECS temperature on the ECS power. The figure shows that the relation is linear. The temperature field is linear with the power of the heat source.

consists of four curves, representing experiments with $I_E = 0.5\,\text{mA}$, $1\,\text{mA}$, $1.5\,\text{mA}$ and $2\,\text{mA}$. It can be seen from the figure that the AE signal remains constant initially as P_T increases. In this regime, the slider is actively flying on the disk without making contact. Then at a certain point, the AE signal suddenly rises. This is when the slider starts to make contact with the highest asperities of the disk. As P_T continues to increase, the contact becomes more intense, and the mode shape of the slider's vibration may also change.[26] Then the AE signal reaches a peak value before it starts to decrease. This peak is defined here as the contact point where $d_{HD} = 0$. It can also be seen that when ω is fixed, the AE signal curves at different I_E have similar shapes. This means that the thermal deformation caused by the ECS heating is minimal and does not affect the slider's fly-height.[18,27]

Figs. 3(d)(e)(f) show the total ECS temperature increase, θ_E, vs P_T. The organization of the figures is the same as those of the AE signal. The vertical dashed lines in each figure represent the position of the contact point. It can be seen from the figures that the curves

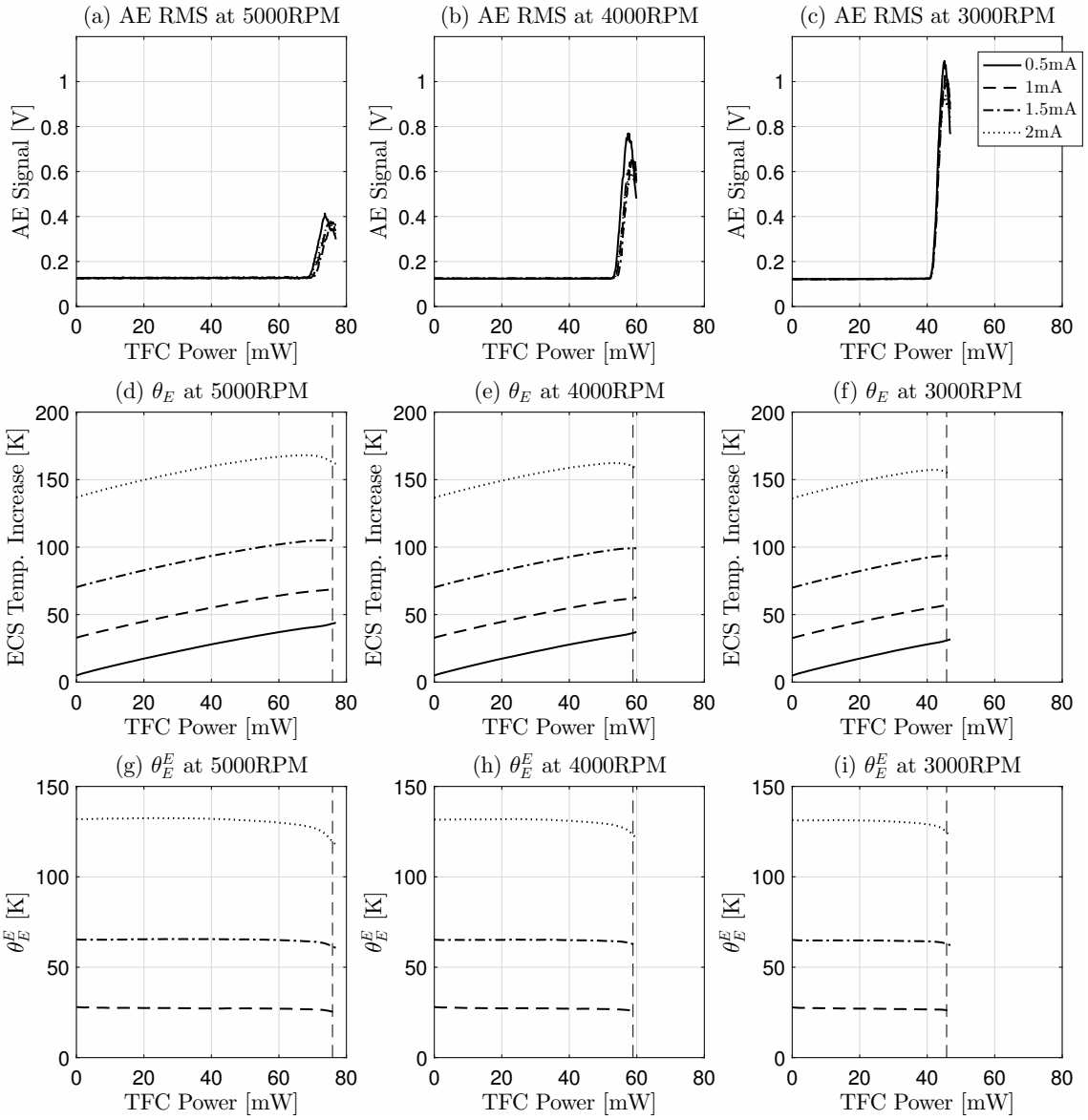

FIG. 3: (a), (b) and (c) show the AE sensor signal versus the TFC power at different ECS currents and disk rotating speeds. The ECS temperature increases as the TFC power increases at different ECS currents and disk rotating speeds. (d), (e) and (f) show the temperature increase of the ECS versus the TFC power of the corresponding experiments. (g), (h) and (i) show the temperature increase of the ECS due to the self ECS heating effect. 10 mW of TFC power increase is equivalent to about 1 nm decrease of head-disk spacing. The legend is the same for all figures, as shown in the upper right corner.

start from $P_T = 0$ and the values of θ_E at the starting points are approximately equal to the values in Fig. 2. At these points, there is only ECS self heating. As P_T increases, the curves

tend to go up as a result of increasing TFC heating. The curves end when the head-disk contact occurs. From the curves with $I_E = 0.5\,\mathrm{mA}$, it can be seen that the portion due to the ECS self heating is small compared with TFC heating. As a result, the ECS self heating effect is usually neglected when I_E is low.[28] And these curves can be considered as a result of TFC heating only, called TFC heating curves. However, the ECS heating effect cannot be neglected when $I_E \geq 1\,\mathrm{mA}$. It can be seen that when $I_E \geq 1\,\mathrm{mA}$, the ECS self heating is at least 50% of θ_E. Therefore, θ_E is influenced by both TFC heating and ECS self heating. These curves are called ECS-TFC heating curves. It can also be seen that the curves in each plot are almost parallel to each other. However, the curves differ when the head and the disk are close to the contact point. When $I_E = 0.5\,\mathrm{mA}$, the curve tends to rise with P_T near the contact point; but when $I_E \geq 1\,\mathrm{mA}$, the curve tends to drop near the contact point.

In order to study the effect of ECS heating only, the TFC heating curves (curves with $I_E = 0.5\,\mathrm{mA}$) are subtracted from the ECS-TFC heating curves (curves with $I_E \geq 1\,\mathrm{mA}$), according to Eq. (2). The result of the subtraction is the ECS temperature increase due to ECS heating, θ_E^E, as shown in Figs. 3(g)(h)(i). In these figures, only θ_E^E with $I_E \geq 1\,\mathrm{mA}$ are left. It can be seen that θ_E^E remains constant initially as P_T increases. However, θ_E^E starts to decrease when the head-disk spacing is within 1 nm. This means that when $d_{HD} > 1\,\mathrm{nm}$, there is not much change on the total heat transfer between the ECS and disk. This agrees with the passive-fly experiment. However, when $d_{HD} < 1\,\mathrm{nm}$, the change in this heat transfer is much more significant.

If ω and I_E are fixed, the heat generated by the ECS and brought away by the disk rotation remains unchanged. As a result, the heat flow across the HDI can be assumed to be constant and d_{HD} is the only factor that is changed. Therefore, how θ_E^E changes indicates the change of the heat transfer across the HDI. To exclude the effect of different ECS power, we normalize θ_E^E by

$$\hat{\theta}_E^E = \frac{\theta_E^E}{\theta_{E0}^E}, \tag{3}$$

where θ_{E0}^E is θ_E^E at the point $P_T = 0$. Fig. 4 shows the average $\hat{\theta}_E^E$ over different bias with respect to d_{HD}, where d_{HD} is converted from P_T by the known relationship between them. It can be seen from the figure that as the slider approaches the disk, $\hat{\theta}_E^E$ decreases slowly initially. When $d_{HD} < 1\,\mathrm{nm}$, $\hat{\theta}_E^E$ starts to decrease rapidly. The decrease of $\hat{\theta}_E^E$ is an indication that the heat transfer across HDI becomes stronger. This is a clear indication that

the model for calculating heat transfer across the gap should predict a strong dependence on the width of the gap, especially when $d_{HD} < 1\,\text{nm}$. As $\hat{\theta}_E^E$ decreases more, the correlation between the heat transfer and the gap becomes stronger.

Recent results of thermal modeling in Refs[13–15] show such a strong dependence. It is also noticed that the rate of decrease is different at different ω. $\hat{\theta}_E^E$ decreases more with lower d_{HD} as ω is higher. This is because when the disk rotation speed is higher, the heat transfered from the head to the disk can be brought away by the disk faster, resulting in more significant heat transfer.

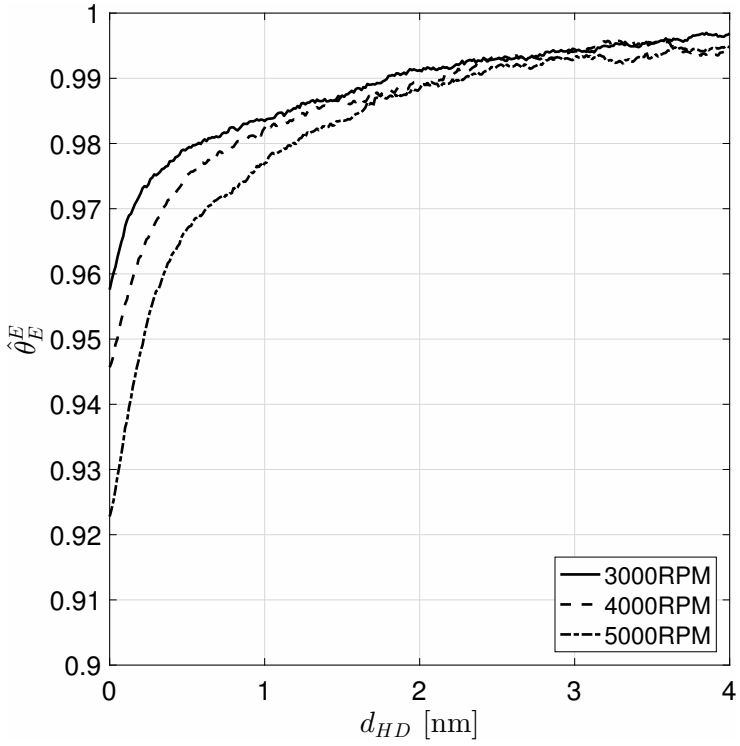

FIG. 4: The average normalized ECS temperature increase due to self heating versus the head-disk spacing at different disk rotation speeds.

Although the experiment was done using PMR heads and disks, the heat transfer mechanism across the HDI remains the same whether the setup uses PMR or HAMR heads and disks. Therefore, the results obtained in the experiment can be directly used to check different heat transfer models for HAMR.

It is interesting to compare the results obtained here on rotating disks and flying heads with the experiment reported in Ref.[17]. There, a slider sat on a stationary disk. The position of the slider was adjusted such that the initial distance between the ECS (called TS in the

	This paper	Ref.[17]
Experimental Setup	Slider flies on rotating disk	Slider sits on stationary disk
Convection Models	Air bearing cooling	Free air convection
Radiation and Conduction Models	Models from Refs.[13–15]	
Convective coefficient[24] [W/(m^2 K)]	$\sim 10^6$	< 100
Conductive and Radiative coefficient[25] [W/(m^2 K)]	$\sim 10^3$ ($d_{HD} = 10$ nm), $\sim 10^6$ ($d_{HD} = 0.5$ nm)	
Total coefficient at $d_{HD} = 10$ nm [W/(m^2 K)]	$\sim 10^6$	$\sim 10^3$
Total coefficient at $d_{HD} = 0.5$ nm [W/(m^2 K)]	$\sim 10^6$	$\sim 10^6$
Total coefficient increase from $d_{HD} = 10$ nm to 0.5 nm	< 10	$\sim 10^3$

TABLE I: The comparison between experiment in this paper and in Ref.[17].

reference) and the disk was 10 to 12 nm. Then the TFC heater (called TA in the reference) was powered on and the temperature of the ECS was measured. The experiment showed that the ECS temperature first increased and then dropped quickly as the TFC power increased. The drop is much steeper than the result shown in Fig. 4. The initial impression might be that the result of this paper and the reference are contradictory. However, it should be noted that the two experiments are under quite different scenarios. A detailed comparison of the two experiments is shown in Table I. It can be seen that when the slider approaches the disk, the heat transfer across the HDI is much larger in the reference. That is the reason why the ECS temperature drops steeper there.

To summerize, an experimental study of the ECS is reported here based on the current HDD design. The study shows that the ECS has a strong self heating effect when it is used with high current bias, and the heating effect is linear with the power of the ECS. It is also shown that the ECS temperature increase due to the self heating decreases with the head-disk spacing. This study indicates that the heat transfer across the HDI is a strong function of the head-disk spacing. The difference between this and a prior experiment is discussed.

This work is supported by the Computer Mechanics Laboratory at the University of California at Berkeley and was funded by Advanced Storage Technology Consortium.

REFERENCES

[1]M. H. Kryder, E. C. Gage, T. W. McDaniel, W. A. Challener, R. E. Rottmayer, G. Ju, Y.-T. Hsia, and M. F. Erden, Proceedings of the IEEE **96**, 1810 (2008).

[2]W. A. Challener, C. Peng, A. V. Itagi, D. Karns, W. Peng, Y. Peng, X. Yang, X. Zhu, N. J. Gokemeijer, Y. T. Hsia, G. Ju, R. E. Rottmayer, M. A. Seigler, and E. C. Gage, Nature Photonics **3**, 220 (2009).

[3]B. C. Stipe, T. C. Strand, C. C. Poon, H. Balamane, T. D. Boone, J. A. Katine, J.-L. Li, V. Rawat, H. Nemoto, A. Hirotsune, O. Hellwig, R. Ruiz, E. Dobisz, D. S. Kercher, N. Robertson, T. R. Albrecht, and B. D. Terris, Nature Photonics **4**, 484 (2010).

[4]B. Xu, Y. T. Toh, C. W. Chia, J. Li, J. Zhang, K. Ye, and C. An, IEEE Transactions on Magnetics **48**, 1789 (2012).

[5]N. Zhou, X. Xu, A. T. Hammack, B. C. Stipe, K. Gao, W. Scholz, and E. C. Gage, Nanophotonics **3**, 141 (2014).

[6]N. Zhou, L. M. Traverso, and X. Xu, Nanotechnology **26**, 1 (2015).

[7]S. Xiong and D. B. Bogy, IEEE Transactions on Magnetics **50**, 148 (2014).

[8]S. Bhargava and E. Yablonovitch, IEEE Transactions on Magnetics **51**, 1 (2015).

[9]H. Wu and D. Bogy, ASME 2016 Conference on Information Storage and Processing Systems , V001T01A003 (2016).

[10]S. Xiong, H. Wu, and D. Bogy, in *SPIE Optical Engineering+ Applications* (International Society for Optics and Photonics, 2014) pp. 920109–920109.

[11]H. Wu, A. R. Mendez, S. Xiong, and D. B. Bogy, Journal of Applied Physics **117**, 17E310 (2015).

[12]L. Chen, D. B. Bogy, and B. Strom, IEEE Transactions on Magnetics **36**, 2486 (2000).

[13]B. V. Budaev and D. B. Bogy, Applied Physics Letters **104**, 061109 (2014).

[14]B. V. Budaev and D. B. Bogy, Journal of Applied Physics **117**, 104512 (2015).

[15]B. V. Budaev and D. B. Bogy, Zeitschrift für angewandte Mathematik und Physik , 1 (2015).

[16]H. Wu, S. Xiong, S. Canchi, E. Schreck, and D. Bogy, Applied Physics Letters **108**, 093106 (2016).

[17]Y. Ma, A. Ghafari, B. V. Budaev, and D. B. Bogy, Applied Physics Letters **108**, 213105 (2016).

[18]J. Li, J. Xu, J. Liu, and H. Kohira, Microsystem Technologies **19**, 1607 (2013).

[19]Y. Shimizu, J. Xu, H. Kohira, M. Kurita, T. Shiramatsu, and M. Furukawa, IEEE Transactions on Magnetics **47**, 3426 (2011).

[20]J. Xu, Y. Shimizu, M. Furukawa, J. Li, Y. Sano, T. Shiramatsu, Y. Aoki, H. Matsumoto, K. Kuroki, and H. Kohira, IEEE Transactions on Magnetics **50**, 114 (2014).

[21]D. Meyer, P. Kupinski, and J. Liu, "Slider with temperature responsive transducer positioning," (1999), uS Patent 5,991,113.

[22]J.-Y. Juang, T. Nakamura, B. Knigge, Y. Luo, W.-C. Hsiao, K. Kuroki, F.-Y. Huang, and P. Baumgart, Magnetics, IEEE Transactions on **44**, 3679 (2008).

[23]J.-Y. Juang and D. B. Bogy, Journal of Tribology (Transactions of the ASME) **129**, 570 (2007).

[24]J.-Y. Juang, Tribology letters **53**, 255 (2013).

[25]Y. Ma, A. Ghafari, B. V. Budaev, and D. B. Bogy, IEEE Transactions on Magnetics **PP**, 1 (2016).

[26]Y.-K. Chen, J. Zheng, and D. B. Bogy, Applied Physics Letters **100**, 243104 (2012).

[27]M. Furukawa, J. Xu, J. Li, K. Hashimoto, and M. Satou, in *ASME 2014 Conference on Information Storage and Processing Systems* (ASME, 2014) p. V001T01A009.

[28]J. Liu, Microsystem Technologies **19**, 1441 (2013).